# Switchable control over in vivo CAR T expansion, B cell depletion, and induction of memory

Sophie Viaud[a], Jennifer S. Y. Ma[a,1], Ian R. Hardy[a,2], Eric N. Hampton[a], Brent Benish[a], Lance Sherwood[a], Vanessa Nunez[a], Christopher J. Ackerman[a], Elvira Khialeeva[a], Meredith Weglarz[a,3], Sung Chang Lee[a], Ashley K. Woods[a], and Travis S. Young[a,4]

[a]Department of Biology, California Institute for Biomedical Research (Calibr), The Scripps Research Institute, La Jolla, CA 92037

Chimeric antigen receptor (CAR) T cells with a long-lived memory phenotype are correlated with durable, complete remissions in patients with leukemia. However, not all CAR T cell products form robust memory populations, and those that do can induce chronic B cell aplasia in patients. To address these challenges, we previously developed a switchable CAR (sCAR) T cell system that allows fully tunable, on/off control over engineered cellular activity. To further evaluate the platform, we generated and assessed different murine sCAR constructs to determine the factors that afford efficacy, persistence, and expansion of sCAR T cells in a competent immune system. We find that sCAR T cells undergo significant in vivo expansion, which is correlated with potent antitumor efficacy. Most importantly, we show that the switch dosing regimen not only allows control over B cell populations through iterative depletion and repopulation, but that the "rest" period between dosing cycles is the key for induction of memory and expansion of sCAR T cells. These findings introduce rest as a paradigm in enhancing memory and improving the efficacy and persistence of engineered T cell products.

CAR T cell | immunotherapy | cancer | control | memory

Chimeric antigen receptor (CAR) T cell therapy has demonstrated durable, complete remissions in patients with hematological malignancies and is rapidly becoming a pillar of cancer immunotherapy (1–4). CAR T cells are engineered by viral transduction of a patient's T cells with genes that encode a synthetic receptor, comprising an extracellular single-chain antibody variable fragment (scFv) connected through a transmembrane domain to costimulatory and CD3ζ signaling domains (5). This enables the T cell to recognize an antigen defined by the specificity of the scFv. To date, most clinical successes with CAR T cell therapy have been achieved by targeting the B cell antigen CD19 in patients with leukemias and lymphomas (1, 2).

A central tenet of this engineering strategy is that the CAR can recapitulate the functions of a native T cell receptor in the ability to autonomously recognize and lyse target cells and induce T cell expansion and differentiation. Although this affords a highly efficacious response, it also creates challenges related to the lack of control over these engineered cells, which can cause toxicities such as cytokine release syndrome and prolonged B cell aplasia in the case of CD19-targeted CAR T cells (6). To address these challenges, we previously described a switchable CAR (sCAR) T cell platform in which the functions of the engineered T cell are controlled by an intermediary antibody-based switch (7, 8). This allows the activation, expansion, and cytokine release of the cells to be dynamically tuned in vitro and in vivo by dosage of the switch. Because the sCAR T cell does not recognize any endogenous antigen in the absence of the switch, it is natively in an "off" or inactive state. This is expected to afford a safer clinical product in patients. However, the long-term phenotypic fate of sCAR T cells, what happens to those cells when the switch is not being dosed, and the impact on B cell populations remain open topics of investigation.

Clinical experience with CD19-targeted CARs has demonstrated that the fate of engineered cells is a critical factor to therapeutic efficacy. CAR T cell products that skew toward a more naïve, persistent central memory (i.e., $T_{CM}$) phenotype have been correlated with sustained remissions in patients with acute lymphoblastic leukemia (6, 9, 10). Accordingly, significant research has focused on achieving CAR T cell populations with this phenotype in vivo through costimulatory domain engineering or by presorting $T_{CM}$ subsets from patients before transduction (10–15). However, memory responses in native T cells are formed through acute, high-load antigen stimulation followed by a "rest" phase, which cannot be recapitulated in current CAR T designs that are constitutively in the "on" state by constantly engaging antigen. The rest phase is important to allow T cell populations to undergo a 1–2-wk contraction in which effector cells that were expanded during stimulation go through apoptosis, resulting in a relative enrichment of the $T_{CM}$ subset. As such, understanding how rest can be leveraged to improve memory formation and engraftment in the context of CAR T cells is expected to lead to more efficacious products.

---

## Significance

Chimeric antigen receptor (CAR) T cell therapy represents a powerful strategy in immuno-oncology. Nevertheless, associated life-threatening toxicities and chronic B cell aplasia have underscored the need to control engineered T cells in the patient. To address these challenges, we have previously developed a switchable CAR (sCAR) T cell platform that allows dose-titratable control over CAR T cell activity by using antibody-based switches. Here, we demonstrate in a syngeneic murine model that the switchable platform can impart antitumor efficacy while dissociating long-term persistence from chronic B cell aplasia. Further, the functional reversibility of the switchable platform can be leveraged to incorporate "rest" phases through cyclical dosing of the switch to enable the induction of a robust central memory population for in vivo, on-demand expansion of sCAR T cells.

---

Here, we exploit a unique feature of the switchable CAR T cell platform that allows cells to rest to recapitulate a physiological period of T cell stimulation that induces robust memory formation (16–20). This work was carried out in a competent immune host as a clinically relevant model to study sCAR T cell efficacy not only against $CD19^+$ B cell lymphoma but also against normal B cells. We developed a syngeneic murine-based switchable CAR T cell platform with murine 4–1BB-based second- and third-generation costimulatory domains that match the human homologs used clinically to promote persistence (1, 10, 21). Costimulatory domains harboring murine 4–1BB were found to be essential in establishing persistence compared with more commonly used CD28-based costimulatory domains and were required to study long-term control aspects. By using these tools, we demonstrate that the switchable system exhibits hallmarks of classical immune regulation in its ability to undergo expansion and contraction of the effector memory compartment when dosed with an anti-CD19 switch. Further, we show that the dosage and timing of the anti-CD19 switch administration can control the amplitude and phenotypic distribution of sCAR T cell expansion. This dynamic, functionally reversible system afforded antitumor control, repopulation of B cells, and physiological-like T cell responses.

## Results

### Development of the Anti-Murine CD19 Switchable CAR T Cell System.
In our previous work (7), we described the development of the switchable system by engrafting a peptide neoepitope (PNE) in the antigen-binding fragment (Fab) region of a targeting antibody (Fig. 1A, gray) and creation of a corresponding sCAR with an scFv that recognized the PNE (Fig. 1A, green). We demonstrated that the switch design, and in particular the site of fusion of the PNE in the Fab, defined the engagement of the immunological synapse between the engineered cell and target cell. This was critical to the activity of human sCAR T cells in a xenograft model. Here, to create a surrogate murine sCAR T cell system, we used an MSGV retroviral vector to transduce mouse splenocytes with an sCAR subcloned into a previously described backbone (8, 22, 23) harboring a murine CD28 costimulatory domain and a modified murine CD3ζ domain with the first and third immunoreceptor tyrosine-based activation motifs (ITAMs) knocked out [28z(1–3); Fig. 2A].

The anti-murine CD19 switch was developed from the Fab (lacking the Fc domain) of the rat clone 1D3. To determine the optimal switch design, the PNE was fused to the N terminus or C terminus of the heavy or light chains of the 1D3 Fab to create a library of six designs (Fig. 1B) (7). In vitro cytotoxicity assays with the use of 1 nM of switch in the presence of an effector-to-target cell ratio of 10:1 of 28z(1–3) sCAR T cells to $CD19^+$ Myc5 target cells demonstrated that the light-chain N-terminally grafted switch (LCNT) exhibited the greatest level of cytotoxicity compared with other switch designs (Fig. 1C). C-terminally grafted switches (HCCT, LCCT, CTBV) exhibited weaker activity, illustrating that the murine system faithfully recapitulated the empirical design concepts of the human sCAR system. Further, LCNT + sCAR 28z(1–3) activity was comparable to that of a conventional CAR T cell [1D3 28z(1–3)], demonstrating that the murine switchable system was capable of conventional CAR T cell level potency in vitro. Therefore, the anti-murine CD19 switch LCNT was used for further studies.

### Generation of Murine sCAR Constructs and in Vitro Potency.
We next optimized the hinge, costimulatory, and activation domains of the sCAR with the intention of developing an sCAR platform that used the 4–1BB-based costimulatory domain similar to those used clinically (10, 24). Nine additional sCAR variants were created and transduced into C3H mouse splenocytes for systematic comparison by in vitro cytotoxicity and cytokine release against the syngeneic $CD19^+$ B cell lymphoma cell line 38c13 (Fig. 2A). The conventional CAR [1D3 28z(1–3)] was used
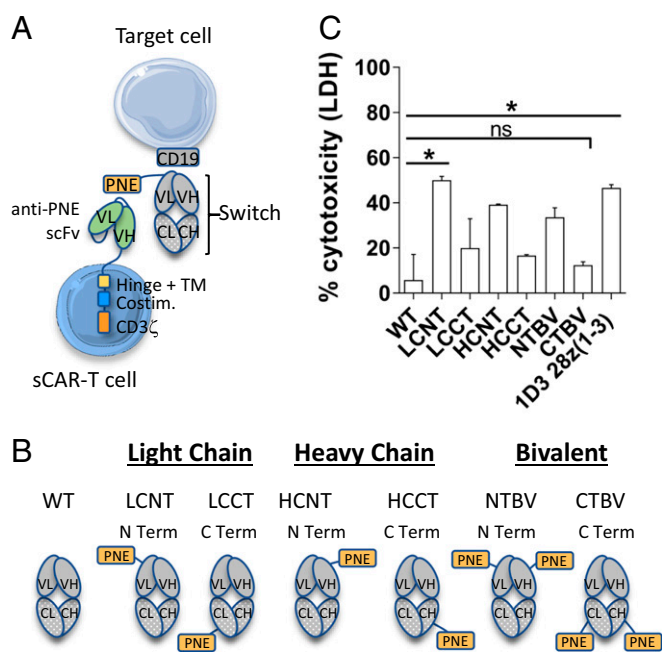






**Fig. 1.** Description of the anti-murine CD19 switchable CAR T platform and in vitro activity of the anti-CD19 switches. (A) Schematic illustration of the switchable CAR T cell system. (B) Schematic diagrams of the anti-mouse CD19 switches. The PNE was grafted on the N terminus (N Term) or C terminus (C Term) of the light chain (LC) or heavy chain (HC) of the anti-mouse CD19 (1D3) switch. Four monovalent switches (LCNT, LCCT, HCNT, and HCCT) and two bivalent switches (NTBV and CTBV) were built, as was a WT switch without peptide as a control. All subsequent in vivo studies were carried out with the anti-mouse CD19 LCNT switch. VL, VH, CL, and CH denote variable light, variable heavy, constant light, and constant heavy chains, respectively, of the Fab depicted. (C) Comparison of switch designs in a cytotoxicity assay based on LDH release. The graph depicts the data from two pooled experiments performed in duplicate. Statistical analyses were performed by Kruskal–Wallis test completed with Dunn's nonparametric multiple comparisons test. Means and SEM are shown (*P < 0.05; ns, not significant).

as our starting point based on our previous work (8) and served as a baseline control throughout.

First, the 36-aa CD28 hinge domain was compared with the shorter 12-aa IgG4m hinge shown to improve activity in human sCAR constructs (7, 25, 26). As shown in Fig. 2B, the IgG4m hinge [Ig-28z(1–3)] afforded significantly higher levels of cytotoxicity and cytokine release (IFN-γ, TNF, and IL-2) in response to specific antigen stimulation in comparison with the CD28-based hinge [28z(1–3)].

Next, the murine CD28-based costimulatory domain was compared with a murine 4–1BB [Ig-BBz(1–3)] or third-generation murine CD28 + 4–1BB [Ig-28BBz(1–3)]-based costimulatory domains by using the IgG4m hinge (Fig. 2A) in the context of CD3ζ with mutated ITAMs. Interestingly, cytotoxicity and cytokine production of the 4–1BB construct were significantly impaired (Fig. 2C). We hypothesized that this may result from the loss of two of three functional ITAMs of the CD3ζ domain. This modification was previously reported to decrease T cell apoptosis and increase in vivo expansion in the context of the CD28 costimulatory domain (27). However, the impact, if any, of a mutated CD3ζ signaling domain in the context of 4–1BB second-generation CAR T cells has not been reported.

To determine if activity could be recovered with an intact (i.,e., WT) CD3ζ, the ITAMs were restored to create the Ig-28z, Ig-BBz, and Ig-28BBz constructs (Fig. 2A). Indeed, cytotoxicity and cytokine release were recovered in the 4–1BB-based construct (Ig-BBz) and cytotoxicity increased in the 28BB construct (Ig-28BBz)
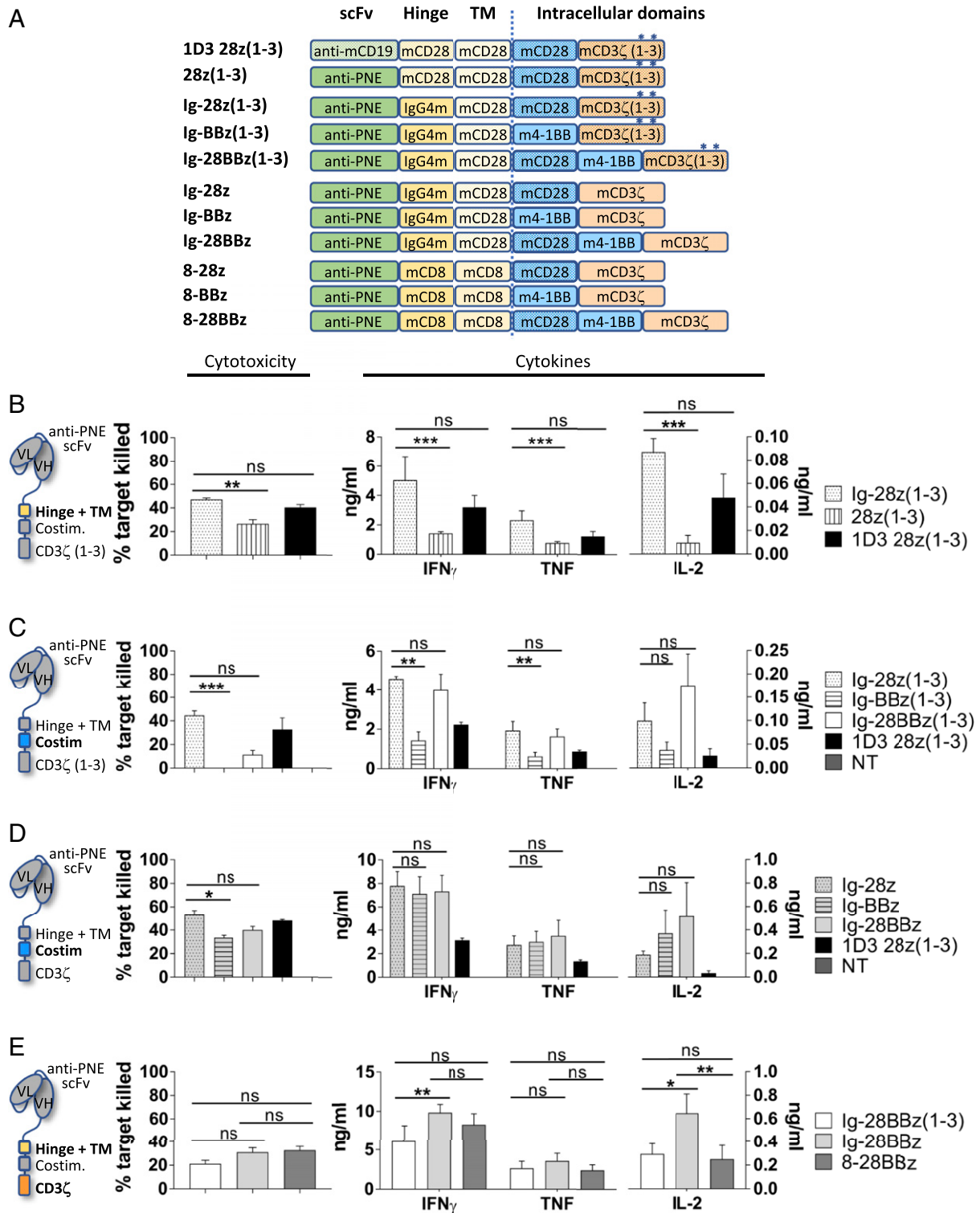
**Fig. 2.** In vitro assessment of sCAR designs. (*A*) Description of the sCAR/CAR designs. Conventional CART-19 is designated as 1D3 28z(1–3). The corresponding sCAR construct 28z(1–3) was based on the same backbone except that the scFv recognizes PNE instead of murine CD19. Second-generation sCAR constructs contained murine CD28 or murine 4–1BB as a costimulation molecule, and third-generation constructs incorporated both. The murine CD28-based hinge was replaced with IgG4m hinge or murine CD8-based hinge. The murine CD3ζ signaling domain was incorporated in its WT form with all three ITAMs intact or with the first and third ITAMs inactivated [CD3ζ(1–3); asterisk]. (*B–E*) Comparison of sCAR T cells based on their cytotoxicity as determined by flow cytometry against 38c13 target cells in the presence of 1 nM anti-mouse CD19 switch and on their cytokine secretion as measured by CBA assay. 1D3 28z(1–3) conventional CAR T cells and nontransduced cells (NT) are used as a reference and a control, respectively. (*B*) IgG4m [Ig-28z(1–3)] vs. CD28-based hinge [28z(1–3)] comparison. (*C*) CD28 [Ig-28z(1–3)] vs. 4–1BB [Ig-BBz(1–3)] vs. CD28 + 4–1BB [Ig-28BBz(1–3)] costimulation domain. (*C* and *D*) WT (z) vs. mutated ITAMs [z(1–3)] in CD3ζ signaling domain. (*E*) Third-generation sCAR comparison based on hinge: IgG4m [Ig-28BBz(1–3) and Ig-28BBz] vs. CD8-based hinge (8-28BBz). All graphs depict the data from two pooled experiments performed in triplicate. Statistical analyses were performed by Kruskal–Wallis test completed with Dunn's nonparametric multiple comparisons test. Means and SEM are shown (*P < 0.05, **P < 0.01, and ***P < 0.001; ns, not significant).

(Fig. 2D). We further confirmed this result by using constructs with a CD8-based hinge (8-28z, 8-BBz, and 8–28BBz), which has been previously validated in second- and third-generation CAR constructs with long-term persistence (28, 29) (*SI Appendix*, Fig. S1C). Comparison of the IgG4m- and CD8-based hinges demonstrated similar levels of cytotoxicity, but with more IL-2 induced in the Ig-28BBz construct (Fig. 2E).

**In Vivo Efficacy and Persistence of Murine sCAR T Cells.** To evaluate sCAR T cell constructs in vivo, we established a syngeneic tumor model by using 38c13 cells s.c. injected into the flank of C3H mice. In this model, untreated mice develop tumors that reach the ethical endpoint within 2 wk after implantation. Tumors were allowed to establish for 7 d, followed by preconditioning animals with 100 mg/kg of cyclophosphamide (CTX) to potentiate the adoptive transfer of CAR T cells as previously described (30, 31). Anti-murine CD19 switch dosing was initiated 4 h after sCAR T cell inoculation and continued every other day for 2 wk, followed by a rest period of 2 wk. The rest period is defined as the time when switch dosing is withheld. Although B cells are being continuously produced, the sCAR T cells are not being activated by switch during this time. This dosing regimen was repeated for three cycles (Fig. 3A).

Three sCAR T cell constructs, all bearing the IgG4m hinge and CD28, 4–1BB, or CD28 and 4–1BB costimulatory domains (Ig-28z, Ig-BBz, and Ig-28BBz), were compared in vivo to assess how the costimulatory domain affected efficacy, B cell depletion, and CAR T cell expansion. Ig-BBz and Ig-28BBz constructs eliminated tumors in all mice, with no relapse up to 152 d (Fig. 3B and *SI Appendix*, Fig. S3B). Notably, neither the Ig-28z nor the 1D3-28z (1–3) CAR effectively controlled tumor growth, despite their superior cytotoxicity compared with BBz or 28BBz constructs in vitro (Fig. 2D). This concurs with previously reported results demonstrating the improved in vivo efficacy of CARs with 4–1BB relative to those bearing CD28 (32, 33).

Analysis of the peripheral blood by flow cytometry revealed that sCAR T cell-treated and control groups [CTX, tumor + CTX, 1D3 28z(1–3)] exhibited B cell depletion 1 wk after CTX treatment (day 15), which rebounded in control groups by day 35, in agreement with previous reports (Fig. 3C and *SI Appendix*, Fig. S3D) (8, 28, 34). Switch dosing in sCAR T cell treatment groups induced complete elimination of B cells after the first cycle of the switch (day 22). B cell populations rebounded when switch dosing was stopped (rest phase to day 35) but were iteratively depleted through the next two switch dosing cycles (days 36–50 and 64–78), thereby demonstrating functional reversibility of activity for the Ig-BBz and Ig-28BBz constructs. B cells returned to levels of untreated controls by day 138 (60 d after last switch dose; Fig. 3C and *SI Appendix*, Fig. S3H) and were accompanied with the restoration of humoral immunity for Ig-BBz and Ig-28BBz by day 153, 2 wk following immunization with ovalbumin (OVA; *SI Appendix*, Fig. S3H). Of note, OVA-specific IgG1 was detectable in the plasma of Ig-BBz and Ig-28BBz mice, but the levels were low compared with CTX-treated mice, probably because of the plasma cells not yet normalized, as B cell levels were comparable.

To understand the impact of switch dosing on Ig-BBz and Ig-28BBz sCAR T cell populations, we also examined sCAR$^+$ T cells in peripheral blood at these time points. Low numbers of sCAR$^+$ T cells were detected in the peripheral blood of Ig-BBz and Ig-28BBz groups through the end of the first dosing and rest cycle (day 35; Fig. 3D and *SI Appendix*, Fig. S3E), putatively as a result of recruitment and recirculation in the secondary lymphoid tissues following CTX-induced lymphopenia and tumor lysis (31). Interestingly, sCAR T cells markedly expanded into a T CD8$^+$ effector/effector memory (T$_{E/EM}$) phenotype after the second and third dosing cycles (Fig. 3E and *SI Appendix*, Fig. S3F). These populations underwent contraction during the rest

phase, but persisted at detectable levels until day 138 (Fig. 3D and *SI Appendix*, Fig. S3E).

To compare the IgG4m vs. CD8-based hinge and the impact of the inactivated ITAMs in CD3ζ, Ig-28BBz was compared with 8–28BBz and Ig-28BBz(1–3), respectively. Both Ig-28BBz and Ig-28BBz(1–3) eliminated tumors in all animals, whereas 8–28BBz and 8-BBz conferred weak antitumor activity (Fig. 3F and *SI Appendix*, Fig. S3 B and G, respectively), in agreement with our prior results demonstrating inferiority of the longer CD8-based hinge (7). However, Ig-28BBz(1–3) and Ig-28z(1–3) failed to eliminate B cells in the second and third dosing cycles (Fig. 3G and *SI Appendix*, Fig. S3 D and G, respectively), which corresponded with an absence of sCAR$^+$ T cells in peripheral blood (Fig. 3 H and I and *SI Appendix*, Fig. S3E). Thus, the costimulatory domain, IgG4m hinge, and CD3ζ (WT) domains were critical to establishing a persistent sCAR T cell population fully controllable by switch dosage.

**Induction and Recall of Memory Responses Using the Switch Dosing Regimen.** We next asked whether the switch dosing regimen could modulate the sCAR T cell phenotype after sCAR T cell engraftment. To create a model in which switch dosing mimicked acute or chronic periods of T cell activation (16, 35), we devised two independent regimens centered on a 28-d cycle: 3 wk of every-other-day dosing followed by 1 wk of rest or 1 wk of every-other-day dosing followed by 3 wk of rest. We compared these with our reference condition of equal periods of dosing and rest (2 wk of dosing, 2 wk of rest). Each of the three regimens was tested with low (0.2 mg/kg) or high (5 mg/kg) doses of the switch (Fig. 4A). Analysis was focused on sCAR T cell phenotype and B cell depletion in the absence of tumor as a readout of sCAR T cell efficacy. The Ig-28BBz sCAR was used because this construct afforded favorable results in the tumor model and most accurately mimicked our human clinical candidate currently in development.

All dosing regimens with Ig-28BBz exhibited B cell depletion after the first week of dosing (day 7; *SI Appendix*, Fig. S4A) in agreement with the aforementioned results. Analysis after 3 wk (day 25) showed that B cells were depleted in 3-wk low and high dosing groups, whereas B cells in the 1- and 2-wk treatment groups (*SI Appendix*, Fig. S4A, *Bottom* and *Top*) exhibited a rebound as a result of the extended rest period between final switch dose and analysis for these groups.

Each group was then resynchronized by the start of the second cycle, on day 28, at which time dosing was initiated in each group. Again, B cells were depleted 1 wk into the second cycle (day 35) with the exception of the 3-wk low-dose group, which exhibited low but detectable levels of B cells, indicating a potentially weaker response for this regimen (*SI Appendix*, Fig. S4A). Remarkably, in the second cycle, the 1-wk high-dose group expanded 385-fold more sCAR$^+$ T cells than the 3-wk high-dose group (Fig. 4B, day 35). At this time point, 1-wk and 3-wk groups had received equal amounts of switch during the second cycle, with the only difference being the duration of dosing in the first cycle and rest period. Expansion in the 1-wk group was further correlated with switch dose level, as the 1-wk high-dose group exhibited 2.6-fold more sCAR$^+$ T cells than the 1-wk low-dose group (Fig. 4B).

Assessment of T cell phenotypes showed that the expanded population was predominantly CD8$^+$ T$_{E/EM}$ cells at day 35 (*SI Appendix*, Fig. S4B). This population underwent a contraction by day 53 (3 wk after the last switch dose for this group) hallmarked by an important reduction in T$_{E/EM}$ but a relative retention of T$_{CM}$ phenotype (Fig. 4 C and D). Notably, the retention of this T$_{CM}$ subset continued to remain higher in the 1-wk group than the 2- or 3-wk treatment groups 40 d after the second cycle was completed (day 74), even without additional switch dosing (Fig. 4D and *SI Appendix*, Fig. S4B). Neither the 3-wk high- nor low-dose groups exhibited detectable peripheral sCAR T cell levels, indicating that
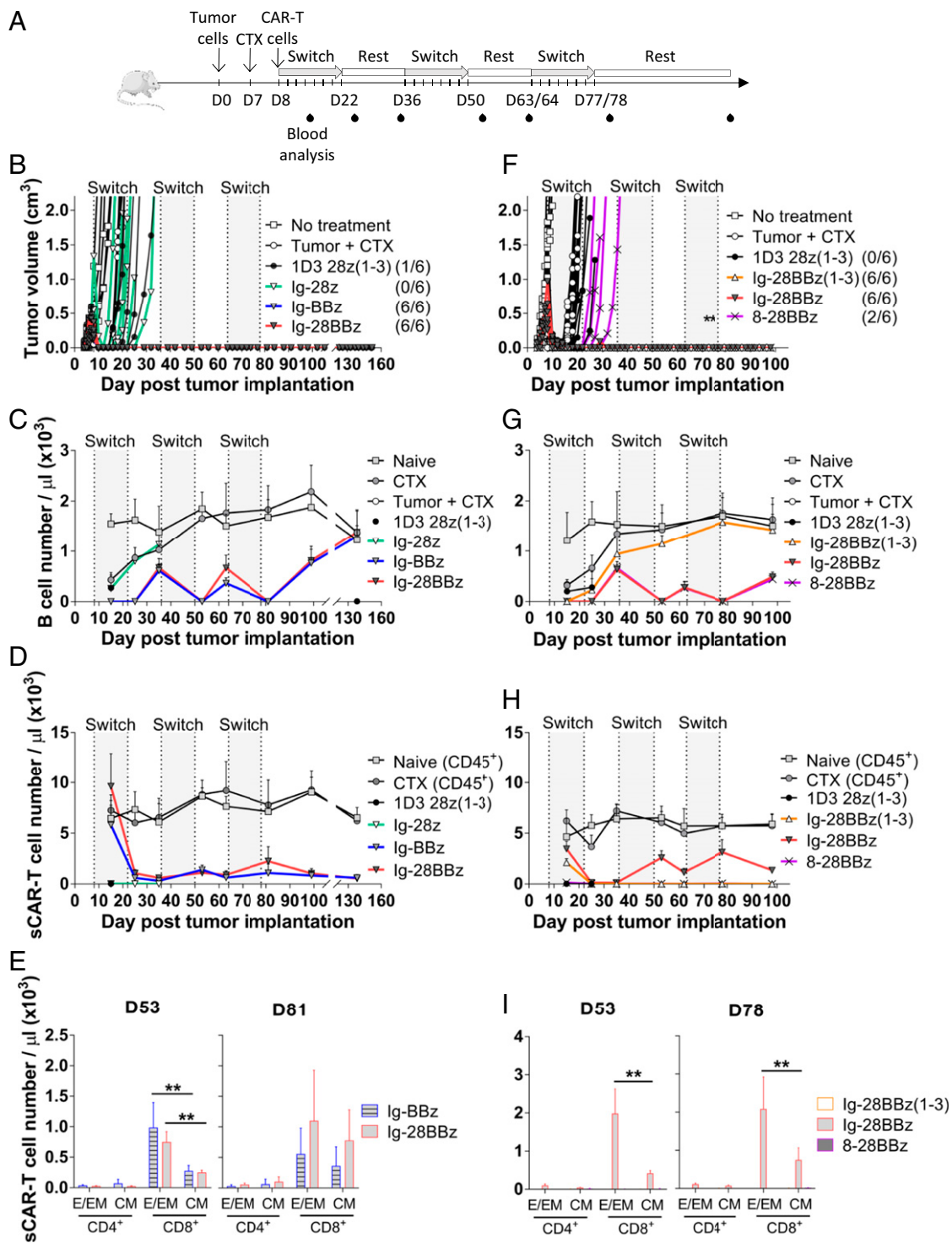
**Fig. 3.** In vivo efficacy and persistence of sCAR designs in a syngeneic murine tumor model. C3H mice were implanted with 38c13 cells at day (D) 0 and preconditioned with CTX at D7. The following day (D8), sCAR/CAR T cells were injected i.v. Anti-murine CD19 switch doses (or PBS solution) were started at D8, D36, and D63/64 for eight doses (gray shading) every other day at 1 mg/kg in a 2-wk on/off (rest) cycle. (*B–E*) This study compared the efficacy of Ig-28z, Ig-BBz, and Ig-28BBz through the evaluation of murine CD28 vs. murine 4–1BB costimulatory molecule. (*F–I*) In this study, Ig-28BBz(1–3), Ig-28BBz, and 8–28BBz were compared to assess IgG4m vs. CD8-based hinge and CD3ζ (WT) vs. CD3ζ(1–3). The 1D3 28z(1–3) was used as a control ($n = 5$–6). (*A*) Experimental design. (*B* and *F*) Tumor growth kinetics of tumor-bearing mice that received no treatment, received CTX only ("Tumor + CTX"), or were administered sCAR/CAR T cells and switch/PBS solution following CTX. The number of tumor-free mice in each treatment group is reported in parentheses. The asterisk indicates, at days 73 and 76, when one mouse each day, in the Ig-28BBz(1–3) group was found dead for unknown reasons. (*C* and *G*) Number of B cells per microliter of peripheral blood over time as determined by flow cytometry. (*D* and *H*) Number of CD45$^+$ cells (naïve and CTX groups) and sCAR/CAR T cells per microliter of peripheral blood over time as determined by flow cytometry. (*E* and *I*) sCAR/CAR T cell phenotype analysis in the peripheral blood by flow cytometry at days 53 and 78/81: CD4$^+$ or CD8$^+$ T effector/effector memory (E/EM; CD44$^+$CD62L$^-$) and central memory (CM; CD44$^+$CD62L$^+$) subsets are indicated. A duplicate experiment combining these two experiments is shown in *SI Appendix*, Fig. S3. Means and SD are shown. Statistical analyses with Mann–Whitney test indicated significant differences at 95% CI (**$P < 0.01$).
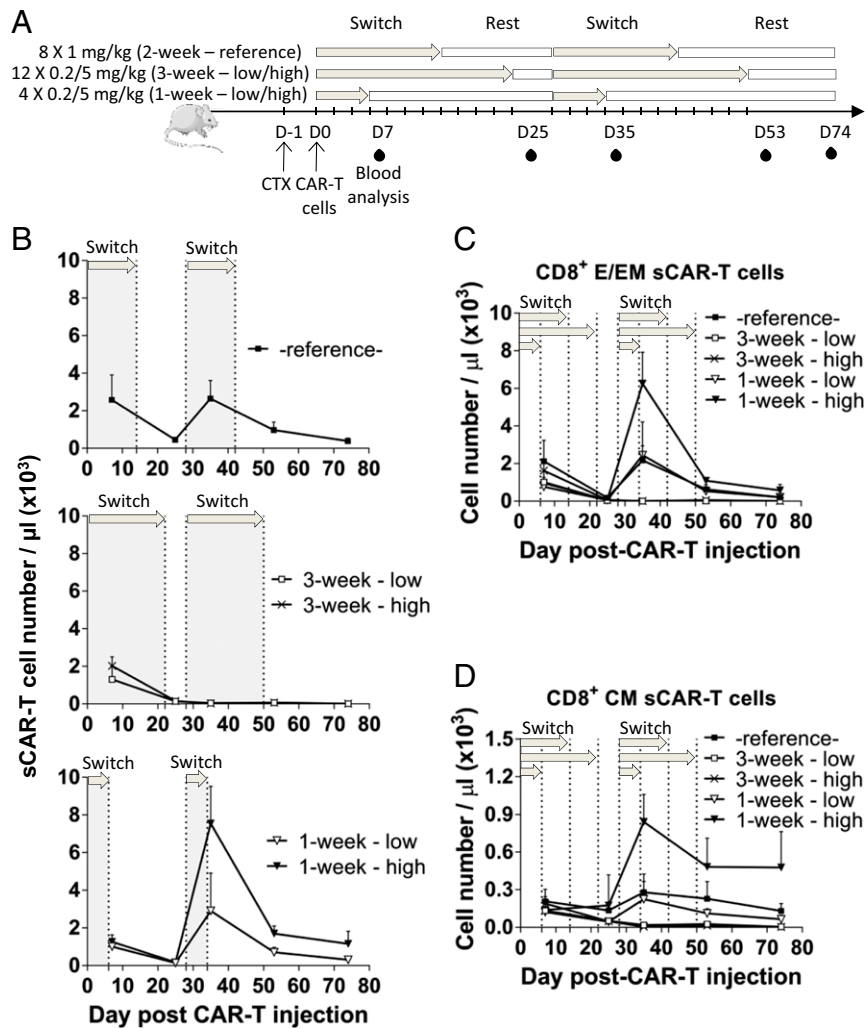
**Fig. 4.** Effect of switch dosing regimens on sCAR T cell expansion and phenotype. C3H mice were preconditioned with CTX and, on the next day, adoptively transferred with Ig-28BBz sCAR T cells. Anti-murine CD19 switch doses were initiated after cell infusion at day (D) 0 and at D28, every other day, in one of three dosing regimens: 2 wk (eight doses) at 1 mg/kg (reference condition used in Figs. 3 and 5), 3 wk (12 doses) at 0.2 and 5 mg/kg (low/high), and 1 wk (four doses) at 0.2 and 5 mg/kg (low/high; gray shading/arrows). Peripheral blood was collected and analyzed for B and sCAR T cells at D7, D25, D35, D53, and D74 ($n$ = 5). (*A*) Experimental design. (*B*) Number of sCAR T cells per microliter of peripheral blood over time as determined by flow cytometry. (*C* and *D*) CD8$^+$ sCAR T cell phenotype analysis in the peripheral blood over time by flow cytometry: (*C*) CD8$^+$ T effector/effector memory (E/EM; CD44$^+$CD62L$^-$) and (*D*) central memory (CM; CD44$^+$CD62L$^+$) subsets. A representative experiment of two experimental replicates is shown. Means and SD are shown.

the duration of the rest phase was more critical to the expansion of the sCAR T cells than the switch dose level.

**Trafficking of the sCAR T Cells in Vivo.** To understand where the sCAR T cells traffic during the expansion and contraction phase, and the extent of B cell depletion in our in vivo studies, we enumerated sCAR T cells present in the spleen, inguinal tumor-draining lymph node (TDLN), and bone marrow (BM) in animals in which tumor was efficiently cleared with Ig-28BBz sCAR T cells and switch (*SI Appendix*, Fig. S5*A*). In this study, we observed an expansion of sCAR T cells ($>3 \times 10^3$ sCAR T cells per microliter) that correlated with undetectable B cells in peripheral blood immediately after the second cycle of switch dosing (day 68; Fig. 5 *A* and *B* and *SI Appendix*, Fig. S5*B*). B cells were also depleted in the spleen, TDLN, and BM, indicating that sCAR T cells and switch were capable of distribution and activity outside peripheral blood. The phenotype of sCAR T cells in blood, spleen, and BM at day 68 was skewed toward an activated CD8$^+$ T$_{E/EM}$ phenotype (Fig. 5*C*). sCAR T cells in the TDLN were mostly CD8$^+$ T$_{CM}$ cells, consistent with migration of T$_{CM}$

cells to secondary lymphoid tissues (35) (Fig. 5*C* and *SI Appendix*, Fig. S5*C*). Importantly, the global pool of sCAR T cells and specifically the number of cells in the sCAR$^+$ CD8$^+$ T$_{CM}$ subset stayed relatively constant in the tissue during the T$_{E/EM}$ contraction phase between day 68 and day 82 (Fig. 5 *B* and *C*) compared with the peripheral blood, where the most drastic changes were observed. These findings were consistent with 2-wk and 4-wk rest periods (Fig. 5 and *SI Appendix*, Fig. S5).

**Discussion**

In this study, we demonstrated the design and engraftment of a switchable, persistent sCAR T cell population with recallable activity that exhibits classical T cell expansion and contraction behavior. To enable the study, we first developed the PNE-based switch and sCAR in a syngeneic murine platform. Consistent with our prior report in the human system (7), the N-terminally designed switch molecule (i.e., LCNT) improved in vitro cytotoxicity and the short IgG4m hinge increased in vivo persistence. These components are expected to shorten the distance between the sCAR T cell and target cell and thereby improve

**Fig. 5.** sCAR T cell trafficking in tissues. 38c13 tumor-bearing C3H mice were treated with CTX before adoptive cell transfer with Ig-28BBz sCAR T cells. Anti-murine CD19 switch injections (or PBS solution) were initiated at day (D) D8 and D51 for eight doses (gray shading) every other day at 1 mg/kg with a 4-wk rest period. Peripheral blood and tissues (spleen, TDLN, BM) were analyzed for B and sCAR T cells at D15, D25, and D35 for blood only and at D68 and D82 for blood and tissues (*n* = 5). (*A*) The experimental design is shown, as well as a graph depicting the number of cells in the peripheral blood over time: B cells (left axis; naïve and CTX only-treated mice and Ig-BB28z mice; dotted line) and sCAR T cells (right axis) in the Ig-28BBz group. (*B*) Number of sCAR T cells (*Top*) and B cells (*Bottom*) per microliter of peripheral blood and in the spleen, TDLN, and BM of the Ig-28BBz–treated mice as determined by flow cytometry at D68 and D82. (*C*) sCAR T cell phenotype analysis in the peripheral blood, spleen, TDLN, and BM by flow cytometry at D68 and D82: CD4$^+$ or CD8$^+$ T effector/effector memory (E/EM; CD44$^+$CD62L$^-$) and central memory (CM; CD44$^+$CD62L$^+$) subsets are shown. The results from one study are depicted. Statistical analyses with Mann–Whitney test indicated significant differences at 95% CI. Data are shown as mean with SD (**$P$ < 0.01 and ***$P$ < 0.001; ns, not significant).

immunological synapse formation that can be decisive for in vivo antitumor activity (7, 26, 36). Because the anti-murine CD19 switch used in these studies was developed from a rat monoclonal antibody, there was a potential for an anti-switch antibody response. This was found in only two animals studied, shown in *SI Appendix*, Fig. S6, which corresponded with the inability to control B cell populations in these outlier animals. In clinical translation, humanization of the antibody is expected to mitigate this potential.

The murine 4–1BB costimulatory domain alone, or in conjunction with the murine CD28 costimulatory domain as a third-generation construct, was essential to achieving control of tumor burden and sCAR T cell persistence in our model. In vivo, sCAR T cell expansion of the 4–1BB-based constructs was predominantly sCAR$^+$ CD8$^+$, which is consistent with reported 4–1BB-driven cytotoxic T cell expansion (37). Expansion was strictly dependent on a fully functional CD3ζ signaling domain in the sCAR construct. This was in contrast to a previous report that demonstrated that inactivation of the first and third ITAMs of CD3ζ can increase expansion of CD28-based constructs in vivo (27). Although CD28 and 4–1BB enhance TCR signaling (38, 39), CD28 stimulation is driven through PI3-kinase-Akt and 4–1BB through TRAF1-2 (40). As CD3ζ also signals through PI3-kinase (41), CD3ζ ITAM functionality could be dispensable in a CAR construct harboring CD28, but not in a 4–1BB-based construct. This is supported by the retention of activity in Ig-28BBz(1–3) in vitro compared with loss of activity for Ig-BBz(1–3) (Fig. 2C). In addition, Ig-28BBz(1–3) sCAR T cells failed to expand in vivo upon repeated stimulation compared with Ig-28BBz, underscoring the importance of CD3ζ ITAMs in the third-generation constructs.

We took advantage of the persistence of the Ig-28BBz sCAR T cells and the expression of CD19 on normal B cells as a target and readout for sCAR T cell efficacy to develop a "self-vaccination/boosting" approach to induce sCAR T cell memory (6). To achieve this, we centered switch dosing regimens around the timing of a natural adaptive immune response to antigen challenge defined by a 1–2-wk activation/expansion phase and a 1–2-wk contraction/death phase (17–20, 35). Use of the antibody Fab domain without the Fc domain in our switch designs provided rapid clearance [expected to be several hours or less (7, 42, 43)] that provided rest phases during which sCAR T cells were not exposed to switch. Expansion kinetics of sCAR T cells dosed for 1 wk followed by 3 wk of rest were in good coherence with these principles, as intense CD8$^+$ sCAR T cell proliferation was observed during the second dosing, superior to all other switch dosing regimen tested (18). Dramatic decreases in the sCAR$^+$ CD8$^+$ T$_{E/EM}$ population during the rest phase was coupled with a persistence of sCAR$^+$ CD8$^+$ T$_{CM}$ cells in secondary lymphoid organs, which may have potentiated the expansion (Figs. 4 C and D and 5C). This resulted in a fivefold increase in the sCAR T cell populations at day 35 than that detected 1 wk after the initial adoptive transfer. These kinetics contrast with conventional CAR T cell kinetics observed in clinical and preclinical models, which exhibit a continuous decay in the numbers of cells after an initial burst of activity (6, 10, 44, 45).

A longer, 3-wk dosing period with short rest was compared with the 1-wk dosing to mimic chronic antigen stimulation (46). This resulted in little to no expansion in the second cycle of switch dosing, in agreement with the principle that persistent overstimulation can cause accumulation of a hyporesponsive population (47, 48). The sCAR$^+$ CD8$^+$ T$_{CM}$ cell population in the peripheral blood remained low for this dosing regimen more than several weeks after dosing, indicating that the initial stimulation period was critical to engraftment of the memory compartment (Fig. 4D). Although B cells remained depleted immediately after the second dosing cycle (day 53), higher PD-1 expression was found on this population, suggesting initial signs of exhaustion (*SI Appendix*, Fig. S4C).

Other approaches to controlling sCAR T cell populations for the purposes of safety and B cell repopulation have included the use of kill switches. These approaches irreversibly eliminate CAR T cells and do not allow for a recall of the response during tumor relapse (49, 50). However, the sCAR T cell platform allows cells to be preserved, and, as we demonstrate here, can be used to promote favorable characteristics in the sCAR T cells through the course of dosing. Further, the sCAR T cell employs a universal design that can be redirected to nearly any therapeutic antigen target. This is expected to be important in combating tumor relapse caused by antigen loss observed with conventional CAR T cell therapy, as long-lived sCAR T cells can then be used to target other B cell antigens such as CD20 or CD22 (7). We expect translation of these results clinically to be a powerful method of promoting antitumor immunity with engineered T cell therapies.

## Materials and Methods

**Mice, Cell Lines, and Murine sCAR T Cells.** Six-week-old female C57BL/6J animals were obtained from Jackson Laboratory (strain 000664), and 6–7-wk-old female C3H mice were obtained from Charles River (C3H/HeN Crl). Mice were housed in a vivarium with a 12-h light cycle and access to food and water ad libitum. All protocols were approved by the institutional animal care and use committee at the Calibr.

Myc5 CD19$^+$ murine B-lymphoma cells (C57BL/6 origin; Myc5 cells overexpressing GFP and CD19) were obtained from Andrei Thomas-Tikhonenko (University of Pennsylvania, Philadelphia, PA). The 38c13, CD19-expressing B cell lymphoma (C3H/HeN origin) was a gift from Ronald Levy (Stanford University, Stanford, CA).

To generate murine sCAR T cells, whole mouse splenocytes were submitted to red blood cell lysis (eBioscience) before being activated for 24 h with 1 μg/mL soluble anti-CD3ε NA/LE antibody (145-2C11), 1 μg/mL anti-CD28 NA/LE antibody (37.51; BD Biosciences), and 60 IU/mL of recombinant human IL-2 (R&D Systems). The activated splenocytes were then retrovirally transduced following a spinoculation protocol by using RetroNectin (Clontech). On the next day, transduced sCAR/CAR T cells were collected, sCAR/CAR expression was assessed by flow cytometry, and cells were directly seeded for expansion at $0.5 \times 10^6$ cells per milliliter with 60 IU/mL of recombinant human IL-2 or enriched for sCAR/CAR T cells (for cytotoxicity assays) before seeding. Cells were used for in vitro or in vivo assays the next day.

**Cytotoxicity Assay by Flow Cytometry.** 38c13 target cells labeled with PKH67 according to the manufacturer's procedure (Sigma-Aldrich) were cocultured at a ratio 1:10 with sCAR and conventional CAR T cells ($1 \times 10^4$ targets with $1 \times 10^5$ effectors) previously CAR$^+$ enriched and normalized (to a $50 \pm 6\%$ transduction efficiency with nontransduced cells; *SI Appendix*, Fig. S1B) and 1 nM anti-mouse CD19 LCNT switch for 6 h at 37 °C. Supernatants were frozen for further analysis, and cells were stained with the Zombie Red Fixable Viability kit (BioLegend) and fixed with 2% paraformaldehyde final (Electron Microscopy Sciences). Five microliters of CountBright Absolute Counting Beads (Molecular Probes) were added to the cells. A fixed volume of samples was acquired on an LSRFortessa X-20 flow cytometer (BD Biosciences) and analyzed by using FlowJo software (version 10.1). The number of viable target cells remaining (Zombie Red$^-$/PKH67$^+$) and beads were used to calculate the number of cells per microliter following the CountBright manufacturer's instructions. The cytotoxicity against the target cells (percentage target killed) was calculated as $100 \times$ [(number of live target cells per microliter in target + effector cells, no switch) − (number of live target cells per microliter in target + effector cells, switch)/(number of live target cells per microliter in target + effector cells, no switch)]. Cytokines in the supernatants were quantified by using Cytometric Bead Array (CBA) Mouse Soluble Protein Flex Set kits (BD Biosciences) according to product manuals after acquisition on an Accuri C6 flow cytometer (BD Biosciences) and analysis with FCAP Array software (BD Biosciences).

**In Vivo Mouse Syngeneic Studies.** C3H mice were implanted s.c. on the flank with $1 \times 10^6$ 38c13 cells in 100 μL PBS solution at day 0. When tumors were measurable at day 7, mice were randomized based on their tumor volume [(length × width$^2$)/2] and were injected with 100 mg/kg i.p. of CTX (Sigma-Aldrich) in PBS solution. On the next day, mice were injected i.v. with $1 \times 10^7$ sCAR/CAR T cells ($30 \pm 6\%$ normalized CAR$^+$, i.e., ~$3 \times 10^6$ CAR/sCAR$^+$ T cells) and, 4 h later, with 1 mg/kg anti-mouse CD19 LCNT switch. This continued every other day for eight doses, followed by a 2-wk resting period, and for a total of three cycles. Control mice (no treatment, CTX only, tumor only,

CTX + tumor) and mice injected with 1D3 28z(1–3) CAR T cells received PBS solution injections to compensate for blood volume changes. Peripheral blood was sampled during the studies at different time points for analysis of the T and B cell populations by flow cytometry. Tumor volume and body weight were monitored during the studies.

For tissue-analysis studies, the experimental setting was as described earlier. Mice were injected with Ig-28BBz sCAR T cells and with a total of two cycles of anti-mouse CD19 LCNT switch doses from day 8 to day 22 and from day 36 to day 50 for one study and from day 51 to day 65 for a second study. Peripheral blood was analyzed at different time points. Spleen, tumor-draining inguinal lymph node, femurs, and tibiae from rear legs were collected from half of the groups after the second cycle of switch at day 53 or day 68 and after a 17-d resting period at day 67 or day 82. After isolation and red blood cell lysis (splenocytes and BM cells), cells were washed, counted with a Vi-Cell XR cell counter, and stained for flow cytometry.

**Statistical Analysis.** All graphs and statistical analyses were generated by using GraphPad Prism software (version 7.01). Data were analyzed by Mann–Whitney test or Kruskal–Wallis test with Dunn's nonparametric multiple comparisons test. Experimental procedures and methods are described in further detail in *SI Appendix, Materials and Methods*.

1. Maude SL, et al. (2018) Tisagenlecleucel in children and young adults with B-cell lymphoblastic leukemia. *N Engl J Med* 378:439–448.
2. Neelapu SS, et al. (2017) Axicabtagene ciloleucel CAR T-cell therapy in refractory large B-cell lymphoma. *N Engl J Med* 377:2531–2544.
3. Mullard A (2017) FDA approves first CAR T therapy. *Nat Rev Drug Discov* 16:669.
4. Anonymous (2018) FDA approves second CAR T-cell therapy. *Cancer Discov* 8:5–6.
5. Dotti G, Gottschalk S, Savoldo B, Brenner MK (2014) Design and development of therapies using chimeric antigen receptor-expressing T cells. *Immunol Rev* 257:107–126.
6. Kalos M, et al. (2011) T cells with chimeric antigen receptors have potent antitumor effects and can establish memory in patients with advanced leukemia. *Sci Transl Med* 3:95ra73.
7. Rodgers DT, et al. (2016) Switch-mediated activation and retargeting of CAR-T cells for B-cell malignancies. *Proc Natl Acad Sci USA* 113:E459–E468.
8. Ma JS, et al. (2016) Versatile strategy for controlling the specificity and activity of engineered T cells. *Proc Natl Acad Sci USA* 113:E450–E458.
9. Klebanoff CA, Gattinoni L, Restifo NP (2012) Sorting through subsets: Which T-cell populations mediate highly effective adoptive immunotherapy? *J Immunother* 35:651–660.
10. Porter DL, et al. (2015) Chimeric antigen receptor T cells persist and induce sustained remissions in relapsed refractory chronic lymphocytic leukemia. *Sci Transl Med* 7:303ra139.
11. Kochenderfer JN, et al. (2009) Construction and preclinical evaluation of an anti-CD19 chimeric antigen receptor. *J Immunother* 32:689–702.
12. Kochenderfer JN, et al. (2015) Chemotherapy-refractory diffuse large B-cell lymphoma and indolent B-cell malignancies can be effectively treated with autologous T cells expressing an anti-CD19 chimeric antigen receptor. *J Clin Oncol* 33:540–549.
13. Kochenderfer JN, et al. (2017) Long-duration complete remissions of diffuse large B cell lymphoma after anti-CD19 chimeric antigen receptor Tcell therapy. *Mol Ther* 25:2245–2253.
14. Sabatino M, et al. (2016) Generation of clinical-grade CD19-specific CAR-modified CD8+ memory stem cells for the treatment of human B-cell malignancies. *Blood* 128:519–528.
15. Wang X, et al. (2016) Phase 1 studies of central memory-derived CD19 CAR T-cell therapy following autologous HSCT in patients with B-cell NHL. *Blood* 127:2980–2990.
16. Wherry EJ, et al. (2003) Lineage relationship and protective immunity of memory CD8 T cell subsets. *Nat Immunol* 4:225–234.
17. Ahmed R, Gray D (1996) Immunological memory and protective immunity: Understanding their relation. *Science* 272:54–60.
18. Carrasco J, Godelaine D, Van Pel A, Boon T, van der Bruggen P (2006) CD45RA on human CD8 T cells is sensitive to the time elapsed since the last antigenic stimulation. *Blood* 108:2897–2905.
19. Homann D, Teyton L, Oldstone MB (2001) Differential regulation of antiviral T-cell immunity results in stable CD8+ but declining CD4+ T-cell memory. *Nat Med* 7:913–919.
20. Pepper M, Jenkins MK (2011) Origins of CD4(+) effector and central memory T cells. *Nat Immunol* 12:467–471.
21. Zhao Z, et al. (2015) Structural design of engineered costimulation determines tumor rejection kinetics and persistence of CAR T cells. *Cancer Cell* 28:415–428.
22. Lee J, Sadelain M, Brentjens R (2009) Retroviral transduction of murine primary T lymphocytes. *Methods Mol Biol* 506:83–96.
23. Kerkar SP, et al. (2011) Genetic engineering of murine CD8+ and CD4+ T cells for preclinical adoptive immunotherapy studies. *J Immunother* 34:343–352.
24. Maude SL, et al. (2014) Chimeric antigen receptor T cells for sustained remissions in leukemia. *N Engl J Med* 371:1507–1517.
25. Jonnalagadda M, et al. (2015) Chimeric antigen receptors with mutated IgG4 Fc spacer avoid fc receptor binding and improve T cell persistence and antitumor efficacy. *Mol Ther* 23:757–768.
26. Hudecek M, et al. (2015) The nonsignaling extracellular spacer domain of chimeric antigen receptors is decisive for in vivo antitumor activity. *Cancer Immunol Res* 3:125–135.
27. Kochenderfer JN, Yu Z, Frasheri D, Restifo NP, Rosenberg SA (2010) Adoptive transfer of syngeneic T cells transduced with a chimeric antigen receptor that recognizes murine CD19 can eradicate lymphoma and normal B cells. *Blood* 116:3875–3886.
28. Davila ML, Kloss CC, Gunset G, Sadelain M (2013) CD19 CAR-targeted T cells induce long-term remission and B cell aplasia in an immunocompetent mouse model of B cell acute lymphoblastic leukemia. *PLoS One* 8:e61338.
29. Sampson JH, et al. (2014) EGFRvIII mCAR-modified T-cell therapy cures mice with established intracerebral glioma and generates host immunity against tumor-antigen loss. *Clin Cancer Res* 20:972–984.
30. Cheadle EJ, Gilham DE, Hawkins RE (2008) The combination of cyclophosphamide and human T cells genetically engineered to target CD19 can eradicate established B-cell lymphoma. *Br J Haematol* 142:65–68.
31. Bracci L, et al. (2007) Cyclophosphamide enhances the antitumor efficacy of adoptively transferred immune cells through the induction of cytokine expression, B-cell and T-cell homeostatic proliferation, and specific tumor infiltration. *Clin Cancer Res* 13:644–653.
32. Milone MC, et al. (2009) Chimeric receptors containing CD137 signal transduction domains mediate enhanced survival of T cells and increased antileukemic efficacy in vivo. *Mol Ther* 17:1453–1464.
33. Kawalekar OU, et al. (2016) Distinct signaling of coreceptors regulates specific metabolism pathways and impacts memory development in CAR T cells. *Immunity* 44:712.
34. Cheadle EJ, et al. (2010) Natural expression of the CD19 antigen impacts the long-term engraftment but not antitumor activity of CD19-specific engineered T cells. *J Immunol* 184:1885–1896.
35. Klebanoff CA, Gattinoni L, Restifo NP (2006) CD8+ T-cell memory in tumor immunology and immunotherapy. *Immunol Rev* 211:214–224.
36. Haso W, et al. (2013) Anti-CD22-chimeric antigen receptors targeting B-cell precursor acute lymphoblastic leukemia. *Blood* 121:1165–1174.
37. Zhang H, et al. (2007) 4-1BB is superior to CD28 costimulation for generating CD8+ cytotoxic lymphocytes for adoptive immunotherapy. *J Immunol* 179:4910–4918.
38. Zhong XS, Matsushita M, Plotkin J, Riviere I, Sadelain M (2010) Chimeric antigen receptors combining 4-1BB and CD28 signaling domains augment PI3kinase/AKT/Bcl-XL activation and CD8+ T cell-mediated tumor eradication. *Mol Ther* 18:413–420.
39. Tammana S, et al. (2010) 4-1BB and CD28 signaling plays a synergistic role in redirecting umbilical cord blood T cells against B-cell malignancies. *Hum Gene Ther* 21:75–86.
40. van der Stegen SJ, Hamieh M, Sadelain M (2015) The pharmacology of second-generation chimeric antigen receptors. *Nat Rev Drug Discov* 14:499–509.
41. Acuto O, Michel F (2003) CD28-mediated co-stimulation: A quantitative support for TCR signalling. *Nat Rev Immunol* 3:939–951.
42. Flanagan RJ, Jones AL (2004) Fab antibody fragments: Some applications in clinical toxicology. *Drug Saf* 27:1115–1133.
43. Adams R, et al. (2016) Extending the half-life of a fab fragment through generation of a humanized anti-human serum albumin Fv domain: An investigation into the correlation between affinity and serum half-life. *MAbs* 8:1336–1346.
44. Garfall AL, et al. (2015) Chimeric antigen receptor T cells against CD19 for multiple myeloma. *N Engl J Med* 373:1040–1047.
45. Grupp SA, et al. (2013) Chimeric antigen receptor-modified T cells for acute lymphoid leukemia. *N Engl J Med* 368:1509–1518.
46. Schietinger A, Greenberg PD (2014) Tolerance and exhaustion: Defining mechanisms of T cell dysfunction. *Trends Immunol* 35:51–60.
47. Chang ZL, Silver PA, Chen YY (2015) Identification and selective expansion of functionally superior T cells expressing chimeric antigen receptors. *J Transl Med* 13:161.
48. Long AH, et al. (2015) 4-1BB costimulation ameliorates T cell exhaustion induced by tonic signaling of chimeric antigen receptors. *Nat Med* 21:581–590.
49. Paszkiewicz PJ, et al. (2016) Targeted antibody-mediated depletion of murine CD19 CAR T cells permanently reverses B cell aplasia. *J Clin Invest* 126:4262–4272.
50. Straathof KC, et al. (2005) An inducible caspase 9 safety switch for T-cell therapy. *Blood* 105:4247–4254.